UNIVERSITY OF CALIFORNIA, SAN DIEGO

Structural and Functional Analysis of Mitochondria in a NASH-HCC Mouse Model

A Thesis submitted in partial satisfaction of the requirements for the degree
Master of Science

in

Biology

by

Kirsten Nicole Malo

Committee in charge:

Professor Gen-Sheng Feng, Chair
Professor Li-Fan Lu, Co-Chair
Professor Gulcin Pekkurnaz

2017

The Thesis of Kirsten Nicole Malo is approved and it is acceptable in quality and form for publication on microfilm and electronically:

_____

_____
Co-Chair

_____
Chair

University of California, San Diego

2017

DEDICATION

I dedicate this Thesis to my parents, Patty and Wilson, for teaching me the importance of hard work and for their continual love and support.

TABLE OF CONTENTS

LIST OF ABBREVIATIONS

C_t	Cycle threshold
DKO	Double knockout
FFAs	Free fatty acids
gDNA	Genomic DNA
HCC	Hepatocellular carcinoma
KO	Knockout
mtDNA	Mitochondrial DNA
NAFLD	Non-alcoholic fatty liver disease
NASH	Non-alcoholic steatohepatitis
PKO	Pten knockout
qPCR	Quantitative polymerase chain reaction
qRT-PCR	Quantitative reverse transcription polymerase chain reaction
ROS	Reactive oxygen species
SKO	Shp2 knockout
WT	Wild-type

LIST OF FIGURES

ACKNOWLEDGEMENTS

First and foremost, I would like to thank Dr. Gen-Sheng Feng for taking me in his lab and being my advisor. I can't express how grateful I am to have had this opportunity. Without him, I don't know where I would be today.

I would also like to thank Dr. Xiaolin Luo for being my mentor and teaching me almost everything I know, as well as providing feedback throughout this project.

Next, I would like to thank all the members of the Feng lab, especially Kaisa Hanley, for their guidance and moral support.

I would also like to thank Dr. Li-Fan Lu and Dr. Gulcin Pekkurnaz for being members of my committee. Dr. Gulcin Pekkurnaz has been an amazing mentor and help to my project, especially the mitochondrial dynamics experiments.

Last but not least, I would like to thank my parents and friends for providing continuous support throughout my whole journey. Without them, I would not have been able to make it this far.

Figures 1 and 2 are a reprint of the material as it appears in Dual Shp2 and Pten Deficiencies□Promote Non-alcoholic Steatohepatitis and Genesis of Liver Tumor-Initiating Cells. Luo, Xiaolin; Liao, Rui; Hanley, Kaisa L.; Zhu, Helen H.; Malo, Kirsten N.; Hernandez, Carolyn; Wei, Xufu; Varki, Nissi M.; Alderson, Nazilla; Chu, Catherine; Li, Suangwei; Fan, Jia; Loomba, Rohit; Qiu, Shuang-Jian; Feng, Gen-Sheng, *Cell Reports*, 2016. The thesis author was a co-author of this paper.

ABSTRACT OF THE THESIS

Structural and Functional Analysis of Mitochondria in a NASH-HCC Mouse Model

by

Kirsten Nicole Malo

Master of Science in Biology

University of California, San Diego, 2017

Professor Gen-Sheng Feng, Chair
Professor Li-Fan Lu, Co-Chair

Hepatocellular carcinoma (HCC) is the second most deadly cancer worldwide, which can result from the progression of fatty liver disease (NAFLD) and steatohepatitis (NASH) to tumorigenesis. NAFLD is an increasing problem in the Western world with the rapid increase in obesity. It is the most commonly diagnosed condition in patients

with liver disorders, and is present in 20-30% of adults in the United States. NASH is a more severe form of NAFLD characterized by inflammation and fibrosis, which can advance to cirrhosis and HCC. Our most recent study to elucidate the molecular mechanisms of HCC showed that two molecules, Shp2 and Pten, have a synergistic effect to prevent hepatocarcinogenesis. The deletion of Shp2 and Pten led to severely fatty livers, early-onset NASH, and tumors. As mitochondria are the major site for fatty acid metabolism and source of ROS, we looked further to address how mitochondrial function is disrupted in this NASH model and whether mitochondrial dysfunction is likely contributing to the progression of NASH to HCC. We quantified the mitochondria and examined mitochondrial functions, including structure, integrity, motility, and gene expression. We show that mitochondrial structure and integrity were compromised in Pten knockout and Shp2/Pten double-knockout mice. Mitochondrial numbers were dramatically decreased in double-knockout mice. We also found that mitochondrial metabolic pathways are dysregulated in Pten knockout mice. These results demonstrate that dysfunctional mitochondria may contribute to the progression of NASH to HCC, and may be a good therapeutic target.

INTRODUCTION

Hepatocellular Carcinoma

Cancer is a major concern worldwide, with over 1 million new cases each year (Siegel et al., 2016). In 2012, about 746,000 deaths were due solely to liver cancer, making it the second deadliest cancer in the world (Theise, 2014). Although death rates for other cancers have decreased in recent years, death from liver cancer has continued to increase (Siegel et al., 2016). Hepatocellular carcinoma (HCC) is the most common form of liver cancer. HCC is predominantly caused by hepatitis B and C infection, obesity, and alcohol use. Other risk factors of HCC include dietary alfatoxins, tobacco use, and diabetes (Yu and Yuan, 2004). Higher incidences of HCC occur in Asian and African countries, where hepatitis B and C are endemic (Chih-Yin Sun and Sarna, 2008). However, in industrialized countries HCC can occur due to increased occurrence of obesity and the progression of a fatty liver to inflammation, scarring, and tumorigenesis (de Alwis and Day, 2008).

Non-alcoholic Fatty Liver Disease and Non-alcoholic Steatohepatitis

The rapid increase of obesity in the Western world has led to increased numbers liver disorders. Non-alcoholic fatty liver disease (NAFLD) is the most commonly diagnosed condition in patients with liver abnormalities (de Alwis and Day, 2008). NAFLD is the accumulation of fat in the liver, not due to alcohol consumption. NAFLD can advance to non-alcoholic steatohepatitis (NASH), which is a more severe form of NAFLD characterized by inflammation, fibrosis, and necrosis. NASH can progress to advanced cirrhosis and then to HCC (Chalasani et al., 2012; Lade et al., 2014), although

the pathogenesis of NAFLD and NASH is not entirely understood (Dowman et al., 2010). Around 12-40% of patients diagnosed with NAFLD will progress to NASH and 15% of those will develop HCC (de Alwis and Day, 2008).

Problems with Current Therapies

Symptoms of hepatocellular carcinoma include pain, weight loss, fatigue, and jaundice, however many patients are asymptomatic, leading to late detection (Chih-Yin Sun and Sarna, 2008). HCC has poor prognosis due to this late-stage diagnosis. The fatality of liver cancer is about 95% (Theise, 2014). Current therapies for HCC involve radiofrequency ablation, transarterial chemoembolization, liver resection, liver transplantation and target-based drugs such as Sorafenib and Regorafenib (Chih-Yin Sun and Sarna, 2008; Llovet et al., 2008). Sorafenib and Regorafenib are multi-kinase inhibitors that target receptor tyrosine kinases that are commonly upregulated in HCC and other cancers. However, these drugs have only been shown to increase survival by three months as compared to no treatment (Chih-Yin Sun and Sarna, 2008; Llovet et al., 2008). These treatments have low survival outcomes due to tumor recurrence and metastasis (Han et al., 2015).

Molecular Signaling Pathways in Hepatocellular Carcinoma

The molecular mechanisms of hepatocellular carcinoma are yet to be fully elucidated, which explains the lack of successful target-based therapeutic developments. Analysis of carcinogenesis in human HCC samples and liver-specific knockout (KO) mouse models has shown the over-activation of classical oncogenes such as β-catenin, c-

Met, and NF-κB (de La Coste et al., 1998; Kaposi-Novak et al., 2006; Pikarsky et al., 2004), or the inactivation of classical tumor suppressors such as p53, RB, p21, and p27 (Zucman-Rossi et al., 2015). In contrast, recent findings have shown that oncogenes such as β-catenin, c-Met, and NF-κB also play an anti-oncogenic role in these mouse models (Zhang et al., 2010; Takami et al., 2007; Maeda et al., 2005). The contradictory findings of different molecules playing dual roles in hepatocarcinogenesis reveal the complexity of HCC. The emerging theory is that the loss of prosurvival molecules causes liver damage, which triggers inflammation, compensatory proliferation and tumorigenesis, although the mechanisms are not clear (Feng, 2012).

Shp2 (PTPN11)

PTPN11 is another gene that shows opposing roles in promoting and suppressing hepatocarcinogenesis. *PTPN11* is the first proto-oncogene found that encodes a cytoplasmic protein tyrosine phosphatase, Shp2 (Chan and Feng, 2007). Shp2 acts to regulate cell survival and proliferation through the activation of the Ras/Erk pathway (Lai et al., 2004). Shp2 was originally identified as a proto-oncogene in leukemia, promoting hematopoietic cell development (Chan and Feng, 2007), however it was recently found that Shp2 plays an anti-oncogenic role in the liver. Liver-specific Shp2 depletion dramatically increased chemically-induced HCC and led to spontaneous tumors after 12 months (Bard-Chapeau et al., 2011). These results were unexpected because previous studies had shown Shp2 having a positive role in cell proliferation and growth in hematopoiesis (Chan and Feng, 2007). Better understanding the molecular interactions

and role of Shp2 in the progression of NASH and HCC will help us find better therapeutic targets.

Shp2 Molecular Interactions

In order to elucidate the pathogenesis of hepatocellular carcinoma, we explored the molecular interactions of Shp2 with another molecule, Pten. Pten is a classical tumor suppressor and a negative regulator of the PI3-K/Akt/mTOR pathway, which is often increased in cancers (Chalhoub and Baker, 2009). Pten deficiency has been found in many types of human cancers, including liver cancer (Galicia et al., 2010). In leukemogenesis, Shp2 antagonizes the tumor-suppressing effect of Pten, showing opposing interactions between the two molecules to suppress hematopoiesis (Zhu et al., 2015). However, we have found that Shp2 and Pten have a synergistic effect in the liver, which leads to early-onset NASH and spontaneous tumors. Mice with liver-specific deletion of Pten and Shp2/Pten exhibited excessive lipid accumulation and free fatty acids (FFAs) in the liver. Levels of reactive oxygen species (ROS) were also markedly increased in Shp2/Pten double knockout mice, suggesting that the progression of NAFLD to NASH and HCC may be from metabolic disorders that cause fat accumulation, leading to oxidative stress and inflammation (Luo et al., 2016).

Mitochondria and HCC

The pathogenesis from NAFLD to NASH requires more than one factor for patients with NAFLD to progress to the inflammation and fibrosis seen in NASH. This is called the “two hits” hypothesis (Day and James, 1998). The first “hit” is the

accumulation of fat in the liver (NAFLD), and the second "hit" are different unknown factors that lead to liver inflammation (NASH) (Fromenty and Pessayre, 2005). It is proposed that the second "hit" may be reactive oxygen species (ROS), which leads to inflammation and fibrosis (Wei et al., 2007). Recent research has shown that the respiratory chain of mitochondria is impaired in NASH patients and leads to increased ROS, suggesting that oxidative stress plays a role in the pathogenesis of NASH (Perez-Carreras et al., 2003). Dysfunctional mitochondria may be a contributing factor in the progression of NASH due to mutations in mitochondrial DNA that encode respiratory chain proteins. This would cause a disruption in the mitochondrial respiration process, leading to increased ROS levels and therefore an increased inflammatory response and fibrosis. As mitochondria are the major site for fatty acid metabolism and source of ROS, we hypothesize that dysfunctional mitochondria play an important role in the progression of HCC by promoting the severe fatty liver phenotype and increased ROS levels.

Experimental Approaches

In this study we will analyze the structure and function of mitochondria in our NASH-HCC mouse model in order to address how mitochondrial function is disrupted in NASH and whether mitochondrial dysfunction is contributing to the progression of NASH to HCC. Our mouse model consists of liver-specific Shp2 knockout (SKO), Pten knockout (PKO), and Shp2/Pten double-knockout (DKO) mice, using wild-type (WT) littermates as controls. This is a good model for NASH and HCC because mice develop early-onset NASH and spontaneous tumors, without the use of chemical carcinogens, mimicking human NASH and HCC. Using our NASH-HCC model, mitochondrial

function will be characterized through structure and integrity. We will then quantify the number of mitochondria in the hepatocytes and measure mitochondrial mobility within the cell. The results of these experiments will allow us to determine if the mitochondria in the NASH mice are dysfunctional. We will also measure the gene expression of mitochondrial metabolic pathways and mitochondrial-encoded gene expression to determine if there is a change in expression, which could indicate that altered mitochondrial gene expression plays a role in the progression of NASH. The results of this study will further our understanding the role of mitochondria in the pathogenesis of NASH to HCC, which could help contribute to finding better therapeutic targets.

MATERIALS AND METHODS

Animals

Hepatocyte-specific Shp2 knockout (SKO, $Shp2^{hep-/-}$:Albumin-Cre^{+}), Pten knockout (PKO, $Pten^{hep-/-}$:Albumin-Cre^{+}), and Shp2 and Pten double-knockout (DKO, $Shp2^{hep-/-}$:$Pten^{hep-/-}$:Albumin-Cre^{+})were generated by Luo et al., 2016. Colonies were maintained by crossing $Shp2^{flox/flox}$:Alb-Cre^{+} mice with $Shp2^{flox/flox}$ mice, $Pten^{flox/flox}$:Alb-Cre^{+} mice with $Pten^{flox/flox}$ mice, and $Shp2^{flox/flox}$:$Pten^{flox/flox}$:Alb-Cre^{+} mice with $Shp2^{flox/flox}$:$Pten^{flox/flox}$ mice. Wild-type (WT, $Pten^{flox/flox}$:$Shp2^{flox/flox}$:Albumin-Cre^{-}) littermates were used as a control. Mice were kept in the vivarium under 12h light/12h dark conditions. All animal experiments were performed in accordance with the protocols (S09108), approved by the UCSD Institutional Animal Care and Use Committee (IACUC).

H&E, Oil-Red-O, and DHE Staining

H&E staining was performed following standard procedures. Oil-Red-O staining was performed using Oil Red O Stain Kit (American MasterTech) according to the instructions of the manufacturer. DHE staining was performed as previously described (Maeda et al., 2005). Briefly, frozen liver sections were stained with 2 μM dihydroethidine hydrochloride (Life Technologies) for 30 minutes at 37 °C.

Electron Microscopy

Mice were euthanized using CO_2. The liver was perfused through the portal vein using 20 ml Hanks' Balanced Salt Solution (HBSS; Gibco) with 10 mM HEPES (Gibco),

followed by 20 ml modified Karnovsky's fixative (2.5% glutaraldehyde, 2% paraformaldehyde, 0.15 M sodium cacodylate buffer, pH 7.4). Liver was extracted, cut into small pieces, and immersed in fixative for 2 hours. After 2 hours, liver was then cut into 1 mm pieces and immersed in fixative for at least 4 hours. Samples were postfixed in 1% osmium tetroxide in 0.15 M cacodylate buffer for 1 hour and stained en bloc in 2% uranyl acetate for 1 hour. Samples were dehydrated in ethanol and embedded in Durcupan epoxy resin (Sigma-Aldrich). Samples were sectioned at 50 to 60 nm on a Leica UCT ultramicrotome and picked up on Formvar and carbon-coated copper grids. Sections were stained with 2% uranyl acetate for 5 minutes, followed by Sato's lead stain for 1 minute. The UCSD Electron Microscopy Facility performed post-fixation. Grids were viewed using a Tecnai G^2 Spirit BioTWIN transmission electron microscope equipped with an Eagle 4k HS digital camera (FEI).

Mitochondrial DNA Content

Total DNA was isolated from 10 mg liver tissue using GenElute Mammalian Genomic DNA Miniprep Kit (Sigma-Aldrich) according to the instructions of the manufacturer. Quantitative polymerase chain reaction (qPCR) was performed using the Mx3005P qPCR System (Agilent) with DyNAmo ColorFlash SYBR Green (ThermoFisher). The primers were designed to target genomic DNA (apoB: 5'-CGT GGG CTC CAG CAT TCT A-3' and 5'-TCA CCA GTC ATT TCT GCC TTT G-3') or mitochondrial DNA (COX1: 5'-TCG CCA TCA TAT TCG TAG GAG-3' and 5'-GTA GCG TCG TGG TAT TCC TGA-3'). To calculate the mitochondrial and genomic DNA content, cycle threshold (C_t) values were related to a standard curve made by cloning the

PCR products into a pDrive vector (Qiagen PCR Cloning Kit). The cloned PCR products were sequence verified. A dilution series with a known number of molecules (5×10^3 to 5×10^6 molecules) was made using spectrophotometry (260 nm). Mitochondrial DNA copy number was calculated as a ratio of mitochondrial DNA to genomic DNA.

Immunoblot Analysis

Immunoblotting was performed following standard protocol. Briefly, proteins were extracted from 30 mg liver tissue and separated by SDS-PAGE. Proteins were transferred to nitrocellulose membranes and incubated in primary antibody overnight at 4 °C, followed by secondary antibody for 1 hour at room temperature. Protein expression was detected by chemiluminescence. Antibodies: COX IV (Abcam), GAPDH (Cell Signaling).

Mitochondrial Motility Assays

Mice were euthanized using CO_2. Primary hepatocytes were isolated by two-step collagenase perfusion, modified from He et al., 2013. The liver was perfused through the portal vein with 50 ml Solution I: HBSS without Ca^{2+} and Mg^{2+}, 10 mM HEPES, 25 mM EGTA, warmed to 37 °C, followed by Solution II: HBSS with Ca^{2+} and Mg^{2+}, 10 mM HEPES, 0.8mg/ml Collagenase Type IV (Gibco), warmed to 37 °C. Liver was extracted and washed in ice-cold phosphate buffered saline (PBS; Sigma-Aldrich). Cells were filtered through a 100 μm cell strainer and centrifuged three times at 50 g for 3 minutes. Cells were resuspended in phenol red-free Dulbecco's Modified Eagle Medium (DMEM; Gibco) supplemented with 10% fetal bovine serum (FBS; HyClone) and

penicillin/streptomycin (Gibco). Cells were plated in 35mm collagen-coated glass bottom dishes (Mattek) at a density of 3 x 10^5 and incubated overnight at 37 °C. Cells were transfected with Mito-DsRed (Clontech) using Lipofectamine 3000 (Invitrogen) and imaged the next day.

Gene Expression Analysis

Total cellular RNA was extracted from 50 mg liver tissue using TRIZOL (Invitrogen). cDNA was generated via reverse transcription using the High-Capacity RNA-to-cDNA Kit (Applied Biosystems). The relative levels of mRNA were determined by quantitative reverse transcription polymerase chain reaction (qRT-PCR), using GAPDH mRNA for normalization. Primers designed for mitochondrial-encoded genes: ATP6 (5'-GCAGTCCGGCTTACAGCTAA-3' and 5'-GGTAGCTGTTGGTGGGCTAA-3'), CYTB (5'-ACCTCCTATCAGCCATCCCA-3' and 5'-AGCGAAGAATCGGGTCAAGG-3'), COX2 (5'-ATAACCGAGTCGTTCTGCCA-3' and 5'-GCTTGATTTAGTCGGCCTGG-3'), ND1 (5'-ATTCGGAGCTTTACGAGCCG-3' and 5'-GGTCAGGCTGGCAGAAGTAA-3'), and RNR2 (5'-ACGAGGGTCCAACTGTCTCT-3' and 5'-AGGTCACCCCAACCGAAAT-3').

RNA-seq

RNA preparation was performed by Dr. Xiaolin Luo. Briefly, total cellular RNA was extracted from liver tissue using the RNeasy Mini Kit (Qiagen). Library preparation

and sequencing were done according to Fox-Walsh et al., 2011. Upstream analysis was done according to Trapnell et al., 2012. Heatmaps were generated by Dr. Gaowei Wang.

Statistical Analyses

Two-tailed student's t test and one-way ANOVA tests were performed. $p < 0.05$ was considered statistically significant.

RESULTS

Shp2 and Pten work synergistically to suppress tumorigenesis

Liver-specific Shp2 knockout (SKO), Pten knockout (PKO), and Shp2/Pten double-knockout (DKO) mice were generated by Luo et al. (2016). Single deletion of only Shp2 or Pten did not cause tumors until 12 months of age. Deletion of both Shp2 and Pten led to spontaneous tumors as early as 5 months and in 100% of mice by 7 months (Figure 1).

Deletion of Shp2 and Pten results in early-onset NASH and high ROS levels

H&E, Oil-Red-O, and DHE staining were performed on liver sections from 2-month-old WT, SKO, PKO, and DKO mice. PKO and DKO mice had extensive lipid accumulation and high levels of free fatty acids (FFAs) (Figure 2, top and middle), showing that PKO and DKO mice developed hepatic steatosis. DHE staining revealed that DKO mice had markedly increased levels of reactive oxygen species (ROS) (Figure 2, bottom).

Mitochondrial integrity is disrupted in PKO and DKO mice

Electron microscopy was done on liver tissue from 3-month-old WT, SKO, PKO, and DKO mice (Figure 3A). The mitochondria in the WT mice were abundant and round, with mitochondrial membranes and cristae intact. The endoplasmic reticulum (ER) was regular and closely associated with the mitochondria. SKO mice had a comparable number of mitochondria to the WT (Figure 3B) and the morphology of the mitochondria was similar, but slightly distorted and less round than in the WT. Both the PKO and DKO

mice had large lipid droplets in the cells, but the DKO had more. The mitochondria in PKO mice were larger and distorted. Some of the mitochondrial membranes were intact, while others were disrupted, although the cristae appear normal. However, there were less mitochondria (Figure 3B) and the ER was slightly disrupted compared to WT. The mitochondria in the DKO mice were large, oblong, and irregularly shaped and there were significantly fewer mitochondria (Figure 3B). Some of the mitochondrial membranes were not intact and the ER was disrupted and not closely associated with the mitochondria. Moreover, the nuclei of the DKO mice were also distorted.

DKO mice have fewer mitochondria

qPCR was used to quantify the number of mitochondria per cell in WT, SKO, PKO, and DKO mice at different ages. SKO mice had slightly decreased mitochondrial numbers compared to wild-type mice at 2 months and 7 months, although it was not statistically significant (Figures 4A & 4B). 12-month-old SKO mice had similar mitochondrial numbers as wild-type mice (Figure 4C). At 7 months, PKO mice had significantly fewer mitochondria than WT (Figure 4B). At 12 months, there was a noticeable reduction in mitochondria, but the difference was not significant (Figure 4C). By 2 months, DKO mice had significantly decreased mitochondrial numbers as compared to WT mice (Figure 4A). At 7 months, both DKO tumor tissue and non-tumor tissue mitochondrial numbers were significantly reduced (Figure 4B). At 12 months, the number of mitochondria in DKO tumor tissue was even more significantly reduced as compared to wild type, and was noticeably decreased as compared to the DKO non-tumor tissue (Figure 4C).

Mitochondrial respiratory proteins are decreased in PKO mice

Western blots were done in 12-month-old WT and PKO mice in order to measure the protein expression of a mitochondrial respiratory protein, cytochrome c oxidase subunit IV (COX IV) (Figure 5). COX IV expression was lower in PKO non-tumor tissue, and even lower in PKO tumor tissue as compared to WT. Expression of COX IV in DKO mice was lower compared to WT, although expression in DKO tumor and non-tumor tissue was similar.

Mitochondrial dynamics are not altered in PKO mice

Hepatocytes were isolated from 2-month-old WT and PKO mice and mitochondria were fluorescently labeled to measure mitochondria motility within the cells (Figure 7). The shape and movement of mitochondria in the WT and PKO cells were comparable. The WT mitochondria appeared somewhat globular, whereas the mitochondria in PKO cells were similar, but slightly longer. The mitochondria showed little movement within both the WT and PKO cells. Of note, the mitochondria in some of the PKO cells were long and tubular, with increased movement compared to the WT. Interestingly, the mitochondria in the PKO cells appeared more interconnected than in the WT cells.

Mitochondrial-encoded gene expression is not significantly altered in SKO, PKO, or DKO mice

qRT-PCR was done using 2-month-old liver tissues to measure the expression of mitochondrial-encoded genes, including cytochrome c oxidase subunit II (COX 2), ATP synthase 6 (ATP 6), NADH dehydrogenase 1 (ND 1), 16S rRNA (Rnr2), and cytochrome b (Cyt B) (Figure 8). SKO mice had slightly increased gene expression and PKO mice had slightly decreased gene expression compared to WT, but the difference was not statistically significant. Notably, DKO mice had comparable gene expression to WT mice, indicating a rescue affect. Cyt B expression was significantly decreased in PKO mice as compared to SKO mice.

Mitochondrial metabolic pathways are dysregulated in PKO mice

RNA-seq was done in order to analyze the gene expression of some metabolic pathways of wild-type (WT) and Pten knockout (PKO) mice from ages 2 months to 16 months. The pathways analyzed include fatty acid oxidation, fatty acid biosynthesis, oxidative phosphorylation, ketone biosynthesis, pyruvate metabolism, amino acid catabolism, and fatty acid transport (Figure 9A). We found that fatty acid biosynthesis and fatty acid transport were significantly upregulated (Figures 9B & 9C), while oxidative phosphorylation and amino acid catabolism were significantly downregulated (Figures 9C &9D) in PKO mice as compared to WT mice (p-value < 0.05). Unexpectedly, oxidative phosphorylation did not have a significant change in gene expression.

DISCUSSION

In this study, we aimed to explore the molecular mechanisms of hepatocellular carcinoma (HCC), in particular to analyze the role of mitochondria in HCC development driven by nonalcoholic steatohepatitis (NASH). We showed that dual deletion of Shp2 and Pten in hepatocytes induced severe NASH, and dramatically accelerated and enhanced hepatocarcinogenesis, indicating their cooperative effects in suppressing liver cancer (Figure 1). Furthermore, we found that livers deficient in Pten or Shp2 and Pten exhibited excessive accumulation of lipids, free fatty acids (FFAs), and reactive oxygen species (ROS) (Figure 2). As mitochondria are the major site for fatty acid metabolism and source of ROS, we looked further to address how mitochondrial function is disrupted in this NASH model and whether mitochondrial dysfunction is likely contributing to the progression of NASH to HCC. We showed that mitochondrial structure and integrity and mitochondrial functions including respiration and metabolic pathways were disturbed in mice at early ages before tumor nodules were observed, suggesting a role in hepatocarcinogenesis.

Electron microscopy of livers from 3-month-old wild-type (WT), Shp2 knockout (SKO), Pten knockout (PKO), and Shp2/Pten double-knockout (DKO) mice was done to assess mitochondrial structure and integrity (Figure 3). The mitochondrial morphology in SKO mice was altered compared to WT. In PKO and DKO mice, there were fewer mitochondria and the mitochondria were larger and distorted. Some of the mitochondrial membranes and the endoplasmic reticulum were disrupted, indicating environmental stress in the cell. The increased stress on these cells may cause increased mitochondrial fusion to fix damaged mitochondria and maximize oxidative capacity (Youle and van der

Bliek, 2012). Increased fusion also explains why there are less mitochondria in the PKO and DKO cells, which is consistent with the decreased number of mitochondria in PKO and DKO cells seen in qPCR (Figure 4).

We quantified the mitochondria in our mice using qPCR to assess whether varying numbers of mitochondria in hepatocytes correlated with increased ROS levels (Figure 4). As early as 2 months of age, DKO mice had significantly less mitochondria than WT mice and PKO mice had significantly fewer by 7 months. By 7 and 12 months of age, the number of mitochondria in DKO tumor tissue was significantly decreased compared to WT. PKO and DKO livers possessed decreased numbers of mitochondria before tumor nodules were observed and tumor cells had fewer mitochondria than normal cells. This suggests that a decrease in the number of mitochondria may contribute to tumorigenesis in these mouse models. The increasing metabolic demand on the mitochondria may contribute to increased ROS production, therefore increasing inflammatory cytokines, compensatory proliferation, and tumorigenesis (Feng, 2012). Mitochondrial dysfunction may lead to increased mitochondrial fusion or mitophagy, which could explain why there are fewer mitochondria (Youle and van der Bliek, 2012). Future experiments should investigate mitochondrial fusion and mitophagy in our NASH-HCC mouse model as these processes may play a role in the change in mitochondrial numbers we have observed and the pathogenesis of NASH.

Cytochrome c oxidase, or complex IV (COX IV) of the respiratory electron transport chain, converts oxygen to water, and thus is important for cellular respiration. The protein expression of COX IV was lower in PKO and DKO tissue, and even lower in PKO tumor tissue (Figure 5). This indicates that there may be a mutation in the gene

encoding COX IV, which is contributing to increased ROS levels in the cell. COX IV transfers electrons to oxygen to create water, so disrupting COX IV could disrupt mitochondrial membrane potential, leading to increased ROS generation (Li et al., 2006). However, it is possible that there is lower COX IV expression because there are fewer mitochondria in PKO and DKO cells (Figure 4). The Western blot was performed using whole liver tissue, rather than isolated mitochondria, so it is necessary to repeat the experiment using isolated mitochondria and to perform qPCR to see if there is a disruption in the respiratory chain or if it is just due to less mitochondria in the cell.

Mitochondrial networks and movement are necessary for normal cell function, so we measured mitochondrial dynamics in WT and PKO cells (Figure 6). However, we did not find any significant difference between WT and PKO cells at 2 months. Overall, there was little mitochondrial movement in both the WT and PKO cells. Some of the PKO cells had mitochondrial networks that were long and tubular, and exhibited more movement than others. This indicates that the high amounts of lipid droplets in PKO cells unexpectedly did not affect the motility dynamics in the cell, although the mitochondrial networks may be affected. The PKO cells may have more extensive and interconnected mitochondria due to increased fusion events. This is consistent with the decreased amount of mitochondria seen in electron microscopy (Figure 3) and quantification (Figure 4).

We measured the expression of genes encoded by the mitochondrial genome to determine if a mutation or change in expression could be contributing to the increased lipid accumulation and ROS production in our mouse model (Figure 7). We found that expression was not significantly altered in SKO, PKO, or DKO mice at 2 months of age.

It is possible that gene expression may be disrupted at later ages. Future studies should analyze later time points to see if gene expression is disrupted as an affect of increased lipid accumulation and ROS levels in the cell.

Several mitochondrial metabolic pathways were altered in PKO mice from 2 months to 16 months of age (Figure 8). Fatty acid biosynthesis was upregulated in PKO mice, which was expected, as there is lipid accumulation in the cells. This is consistent with other studies (Lambert et al., 2014). However, fatty acid oxidation was neither upregulated nor downregulated. We hypothesized that fatty acid oxidation would be upregulated as a mitochondrial compensatory mechanism to reduce the fat content due to increased fatty acid production, which is what others have seen (Iozzo et al., 2010), although these studies were done using other methods. Our results likely explain why there is excessive fat in the PKO livers. Oxidative phosphorylation was significantly downregulated in PKO mice compared to WT. The high amounts of lipid content in the cells may cause damage to the mitochondrial respiratory chain, causing a decrease in the oxidative capacity of the mitochondria. This could also lead to increased mitochondrial fusion, which is consistent with what we saw in electron microscopy (Figure 3) and mitochondrial quantitation (Figure 4).

Amino acid catabolism was also markedly downregulated in PKO mice (Figure 8E). Amino acid catabolism, such as tyrosine metabolism, has been associated with insulin resistance, metabolic syndrome, and diabetes, and these are also associated with NAFLD and NASH. Some research has found dysregulated amino acid metabolism in NAFLD (Jin et al., 2016). It is well known that cancer cells highly metabolize glutamine (King, 2007), so the PKO mice may have increased glutamine catabolism, contributing to

tumorigenesis. Future studies should further closer as to which amino acids are being highly metabolized in PKO mice compared to WT mice.

In this study, we have shown that our Shp2/Pten double-knockout mouse model is a relevant model to human NASH and HCC through its extensive accumulation of lipids and tumor development. We showed that mice with Shp2 and Pten ablation had high ROS levels and that mitochondrial function is disrupted at early ages, even before tumors nodules were observed, suggesting that dysfunctional mitochondria play a role in hepatocarcinogenesis. In the future, we would like to continue to explore mechanistically how mitochondria are driving tumorigenesis through the interactions that Shp2 and Pten have with mitochondria. This will further our understanding the role of mitochondria in the pathogenesis of NASH to HCC, which could help contribute to finding better therapeutic targets.

FIGURES

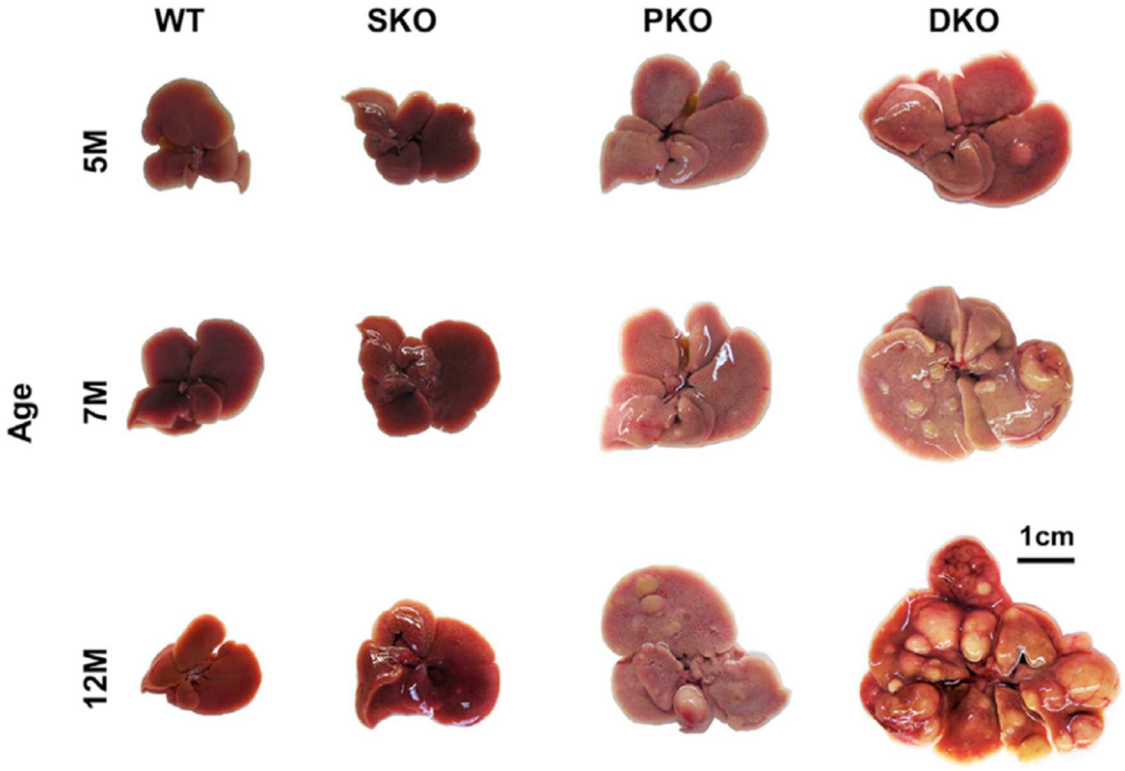

Figure 1. Shp2 and Pten work synergistically to suppress liver tumorigenesis. Macroscopic view of livers from 5-month-old, 7-month-old, and 12-month-old WT, SKO, PKO, and DKO mice.

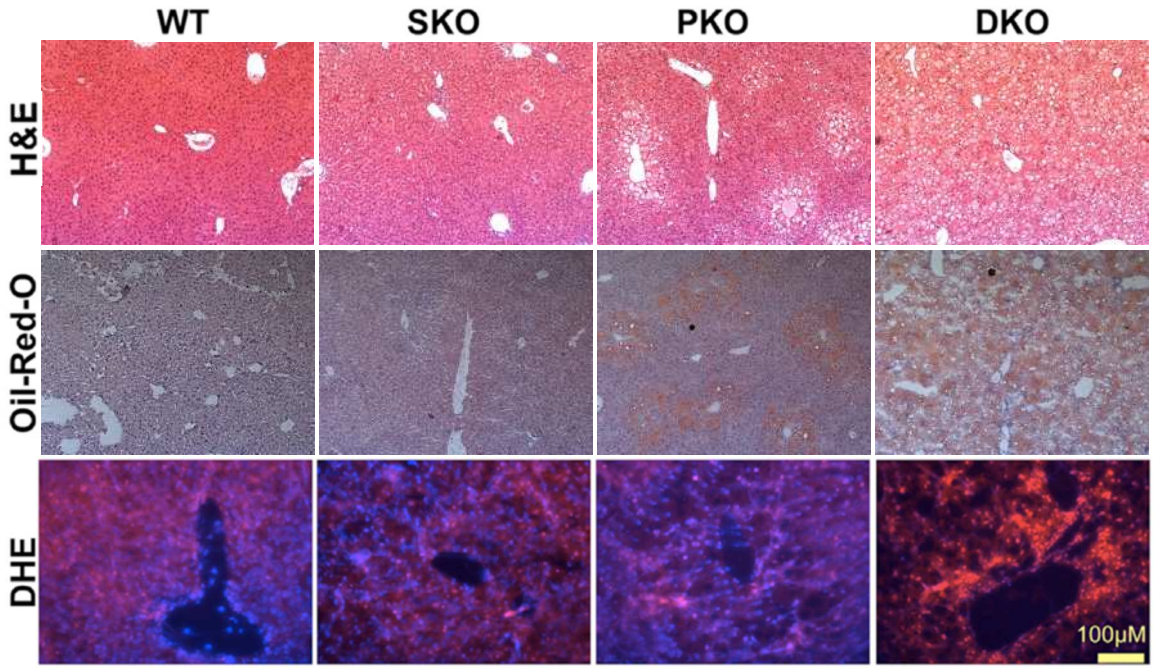

Figure 2. Deletion of Shp2 and Pten results in early-onset NASH and high ROS levels. H&E, Oil-Red-O, and DHE staining of liver sections from 2-month-old WT, SKO, PKO, and DKO mice.

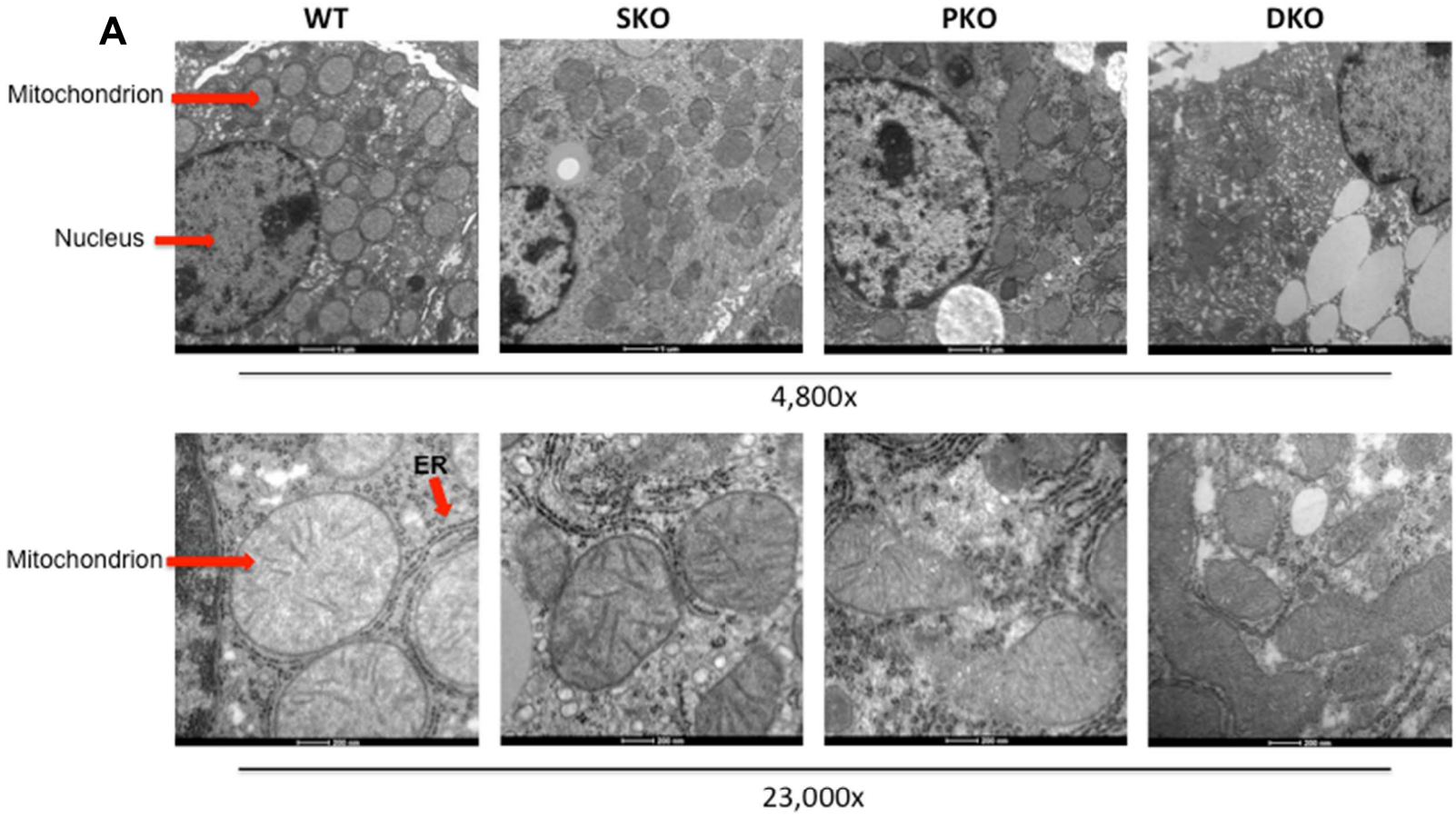

Figure 3. Mitochondrial integrity is disrupted in PKO and DKO mice. (**A**) Electron microscopy of 3-month-old WT, SKO, PKO, and DKO mice. Mitochondria, endoplasmic reticulum (ER), and nuclei are labeled. (**B**) Quantification of the number of mitochondria per cytoplasmic area per cell. * indicates $p < 0.05$ versus wild-type control and ** indicates $p < 0.01$ versus wild-type control.

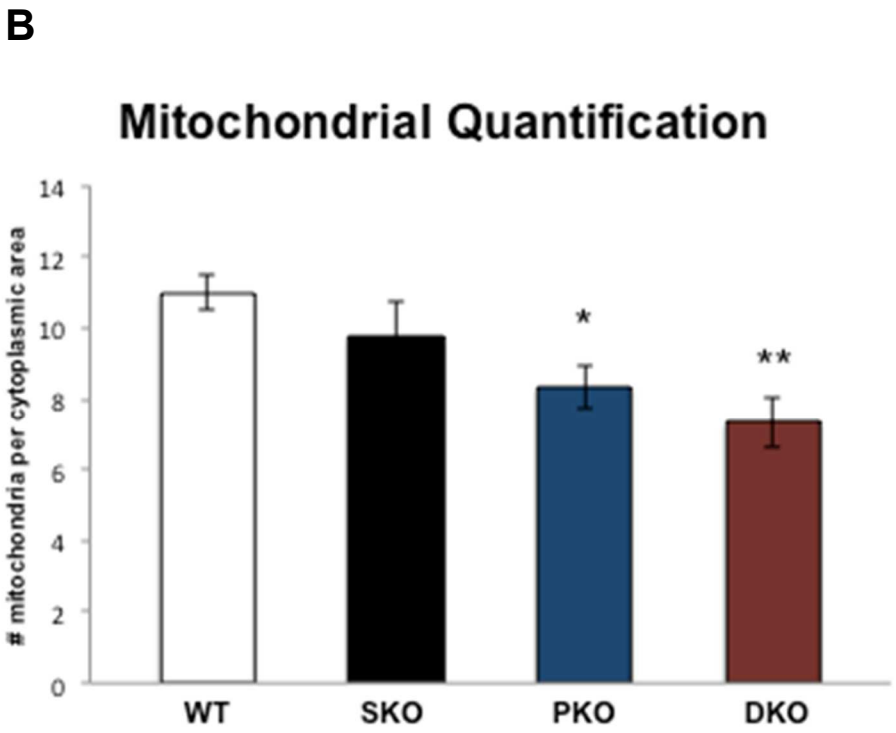

Figure 3. Mitochondrial integrity is disrupted in PKO and DKO mice. (**A**) Electron microscopy of 3-month-old WT, SKO, PKO, and DKO mice. Mitochondria, endoplasmic reticulum (ER), and nuclei are labeled. (**B**) Quantification of the number of mitochondria per cytoplasmic area per cell. * indicates $p < 0.05$ versus wild-type control and ** indicates $p < 0.01$ versus wild-type control, continued.

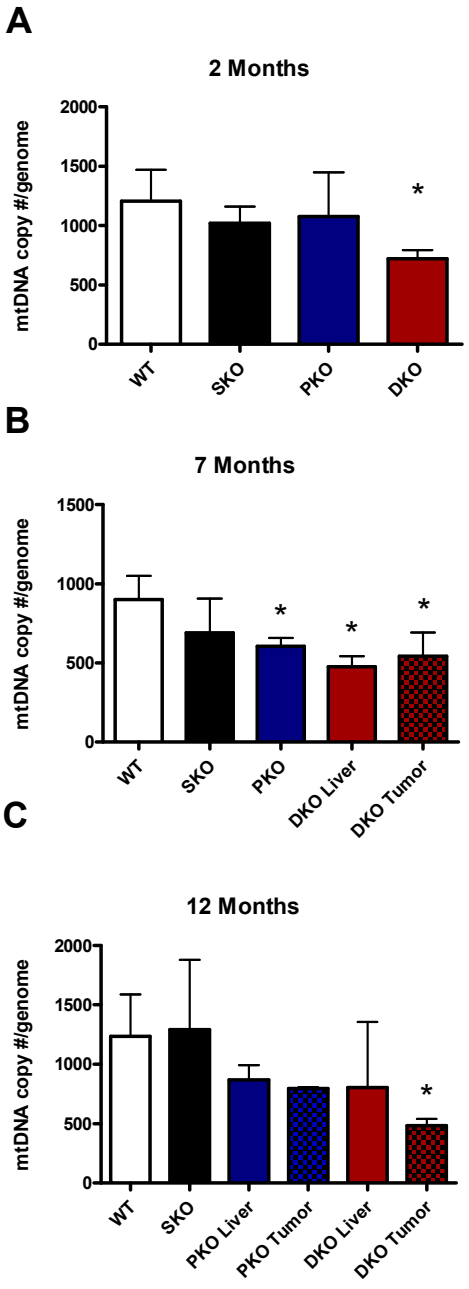

Figure 4. DKO mice have fewer mitochondria. Mitochondrial DNA and nuclear DNA copy numbers were determined using qPCR by comparing cycle threshold (C_t) values to a standard curve. Mitochondrial numbers were calculated as a ratio of mtDNA to genomic DNA for (**A**) 2-month-old, (**B**) 7-month-old, and (**C**) 12-month-old WT, SKO, PKO, and DKO mice (n=3 mice per group). Data are shown as means ± SD. * indicates $p < 0.05$ versus wild-type control.

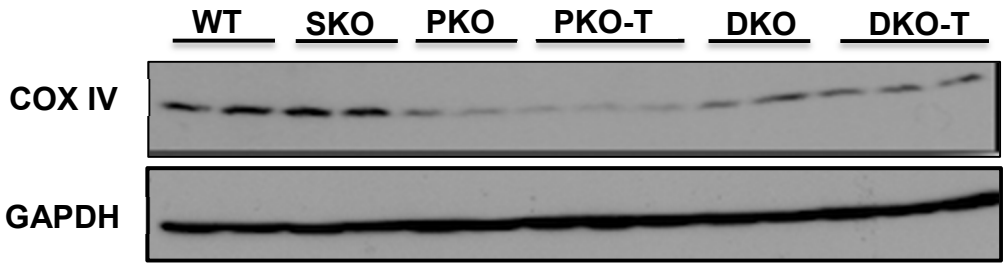

Figure 5. Mitochondrial respiratory proteins are decreased in PKO mice. Immunoblot analysis of COXIV in WT, SKO, PKO non-tumor, PKO tumor, DKO non-tumor, and DKO tumor liver tissues from 12-month-old mice.

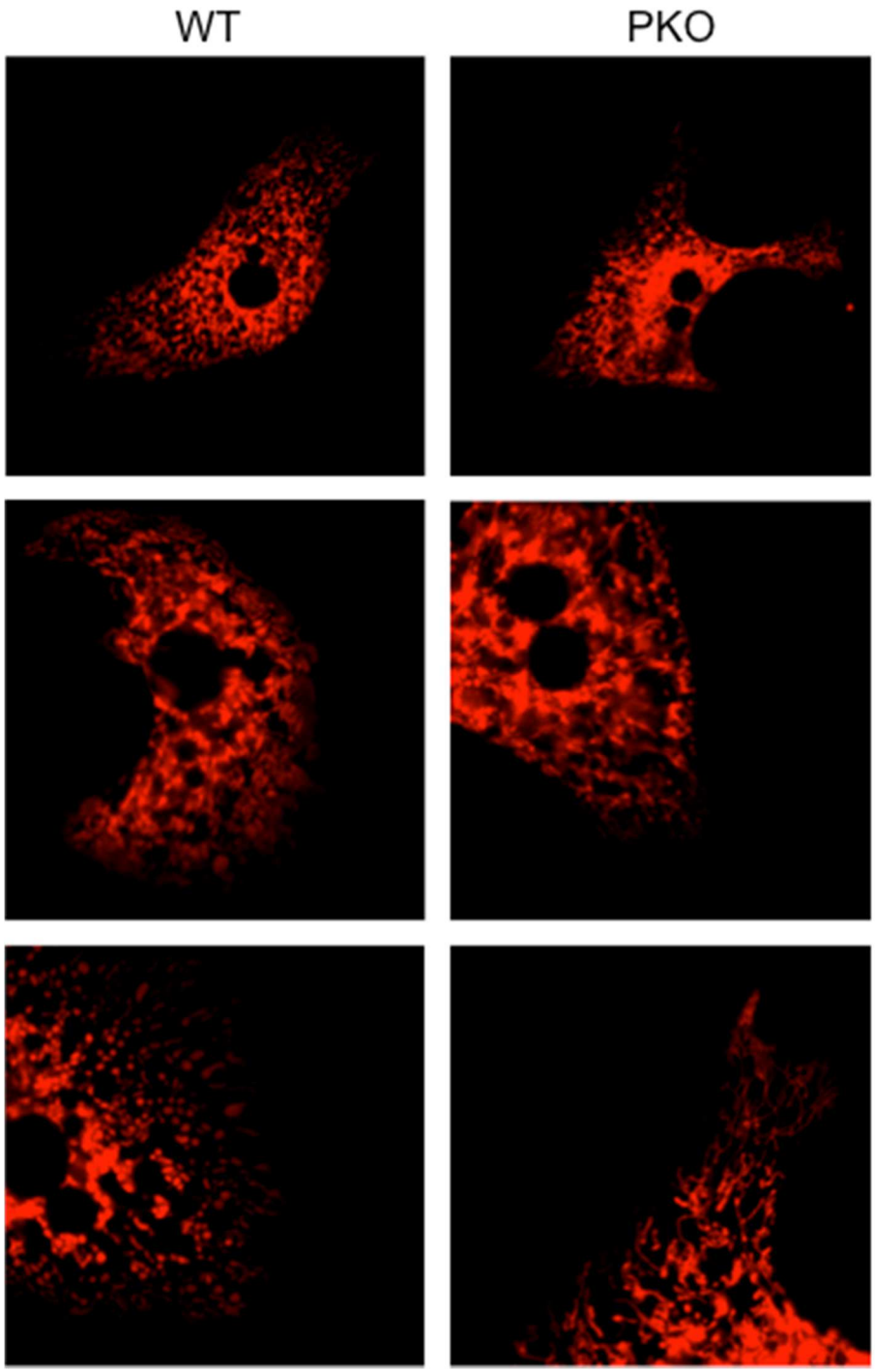

Figure 6. Mitochondrial dynamics are not altered in PKO mice. Primary hepatocytes were isolated from 2-month-old WT and PKO mice. Mitochondria were fluorescently labeled using Mito-DsRed.

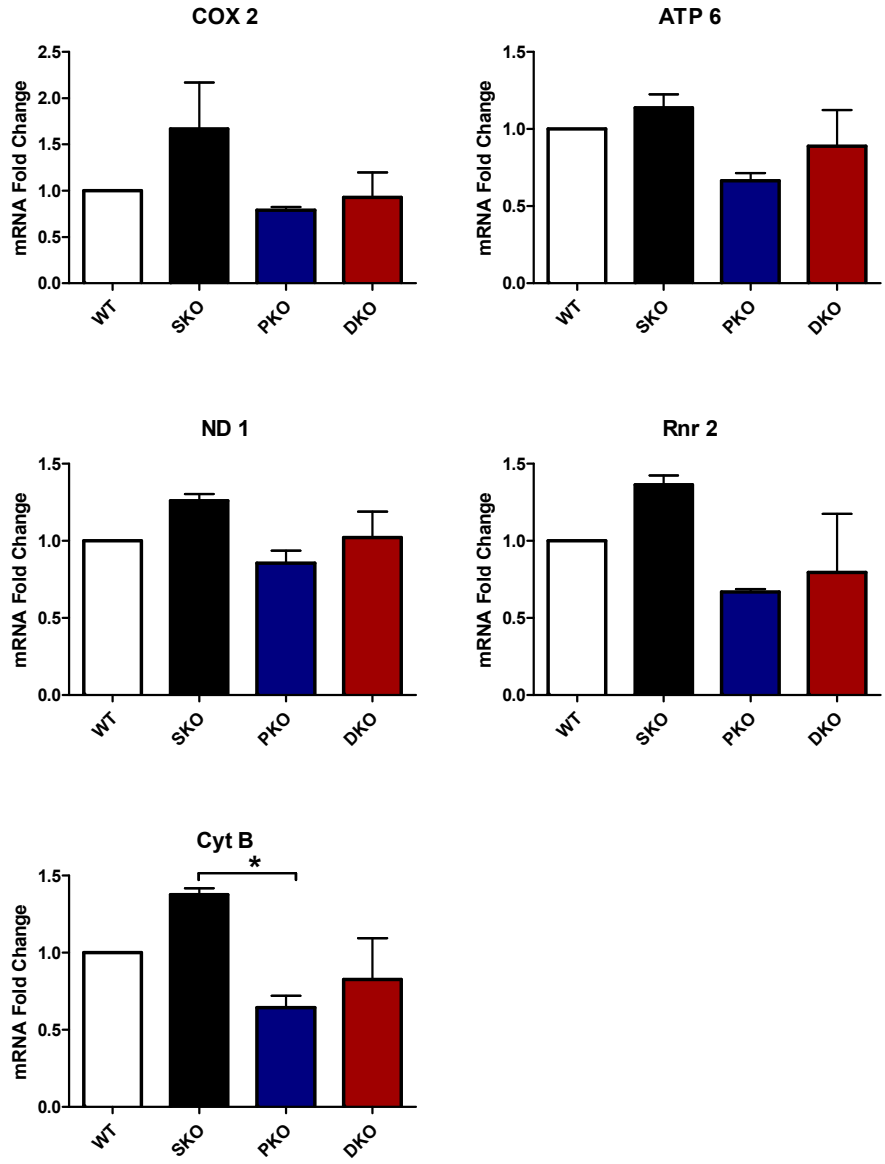

Figure 7. Mitochondrial-encoded gene expression is not significantly altered in SKO, PKO, or DKO mice. COX 2, ATP 6, ND 1, Rnr2, and Cyt B gene expression were measured using qRT-PCR (n=3 mice per group). GAPDH was used as a control. Data are shown as means ± SD. * indicates $p < 0.05$.

A

Pathway	Score	High P	Low P
Fatty acid oxidation	-0.0579522	0.589	0.411
Fatty acid biosynthesis	0.42178834	0.04	0.96
Oxidative phosphorylation	-0.2931519	0.951	0.049
Ketone biosynthesis	-0.118632	0.697	0.303
Pyruvate metabolism	0.28279595	0.083	0.917
Amino acid catabolism	-0.7960941	1	0
Fatty acid transport	0.30636424	0.044	0.956

Figure 8. Mitochondrial metabolic pathways are dysregulated in PKO mice. RNA-seq analysis of mitochondrial pathways in WT and PKO mouse livers ages 2 months to 16 months. (**A**) Shows the list of metabolic pathways. Score represents relative gene expression, with a positive value indicating upregulation and a negative value indicating downregulation. High P or Low P value < 0.05 denotes gene expression is significantly upregulated or downregulated, respectively. Mitochondrial pathways that were significantly altered include (**B**) fatty acid biosynthesis, (**C**) fatty acid transport, (**D**) oxidative phosphorylation, and (**E**) amino acid catabolism. Relative gene expression is depicted by a gradient, with green representing lowest gene expression (-3) and red representing highest gene expression (+3). Genes involved in the pathway are listed to the right of the graph.

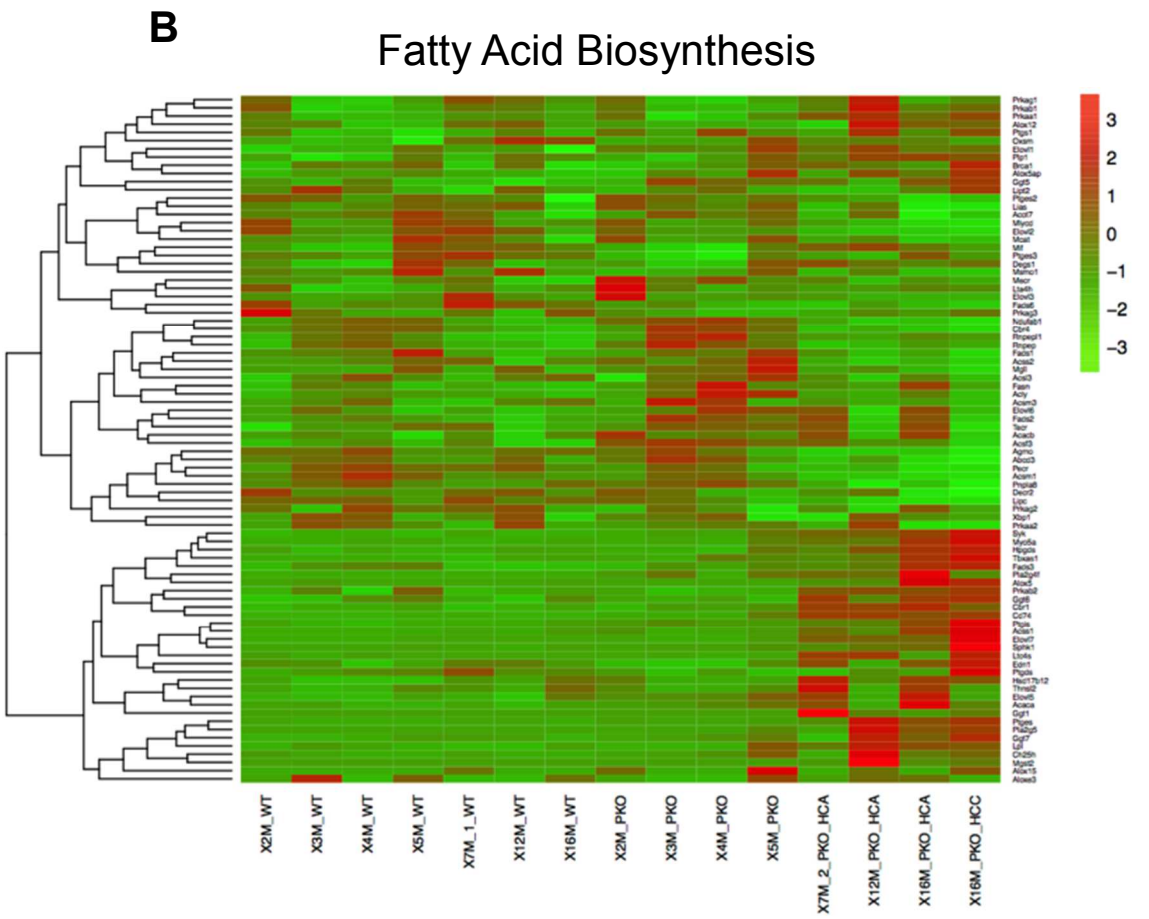

Figure 8. Mitochondrial metabolic pathways are dysregulated in PKO mice. RNA-seq analysis of mitochondrial pathways in WT and PKO mouse livers ages 2 months to 16 months. (**A**) Shows the list of metabolic pathways. Score represents relative gene expression, with a positive value indicating upregulation and a negative value indicating downregulation. High P or Low P value < 0.05 denotes gene expression is significantly upregulated or downregulated, respectively. Mitochondrial pathways that were significantly altered include (**B**) fatty acid biosynthesis, (**C**) fatty acid transport, (**D**) oxidative phosphorylation, and (**E**) amino acid catabolism. Relative gene expression is depicted by a gradient, with green representing lowest gene expression (-3) and red representing highest gene expression (+3). Genes involved in the pathway are listed to the right of the graph, continued.

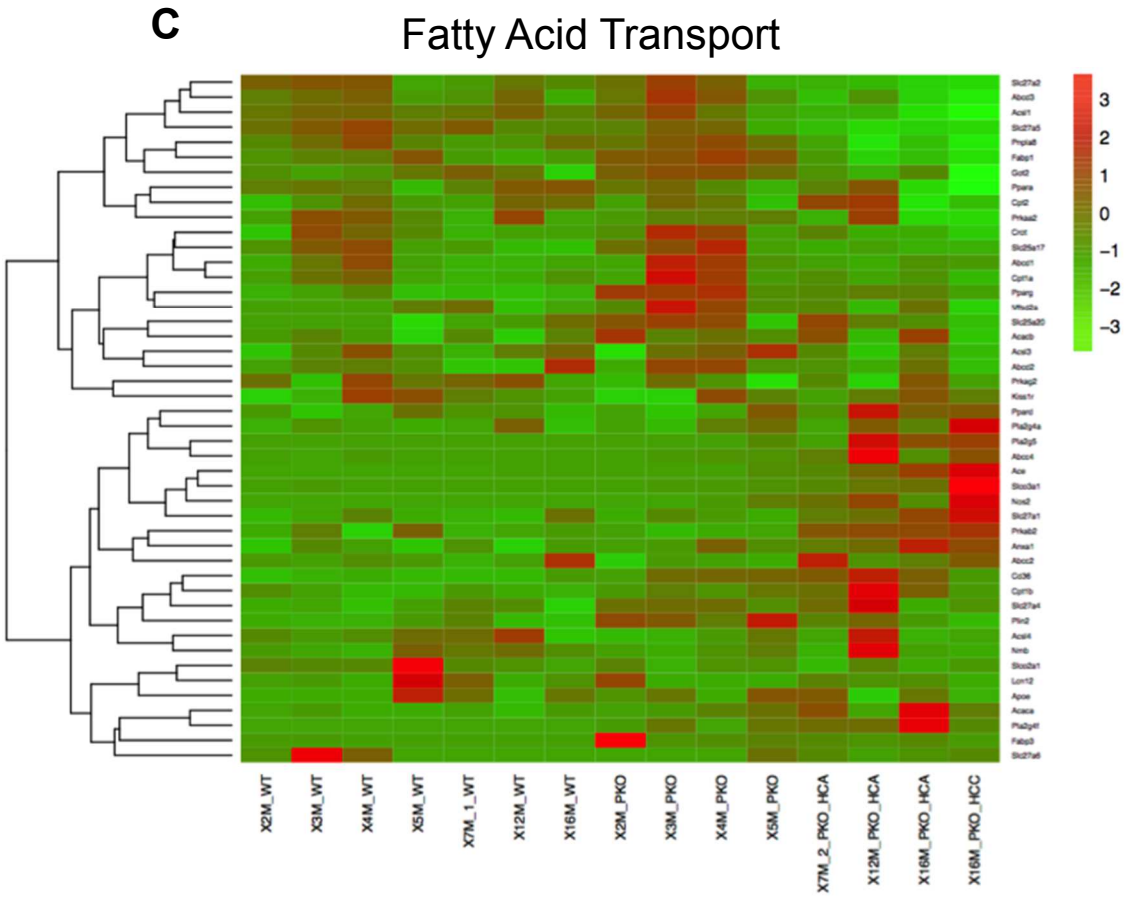

Figure 8. Mitochondrial metabolic pathways are dysregulated in PKO mice. RNA-seq analysis of mitochondrial pathways in WT and PKO mouse livers ages 2 months to 16 months. (**A**) Shows the list of metabolic pathways. Score represents relative gene expression, with a positive value indicating upregulation and a negative value indicating downregulation. High P or Low P value < 0.05 denotes gene expression is significantly upregulated or downregulated, respectively. Mitochondrial pathways that were significantly altered include (**B**) fatty acid biosynthesis, (**C**) fatty acid transport, (**D**) oxidative phosphorylation, and (**E**) amino acid catabolism. Relative gene expression is depicted by a gradient, with green representing lowest gene expression (-3) and red representing highest gene expression (+3). Genes involved in the pathway are listed to the right of the graph, continued.

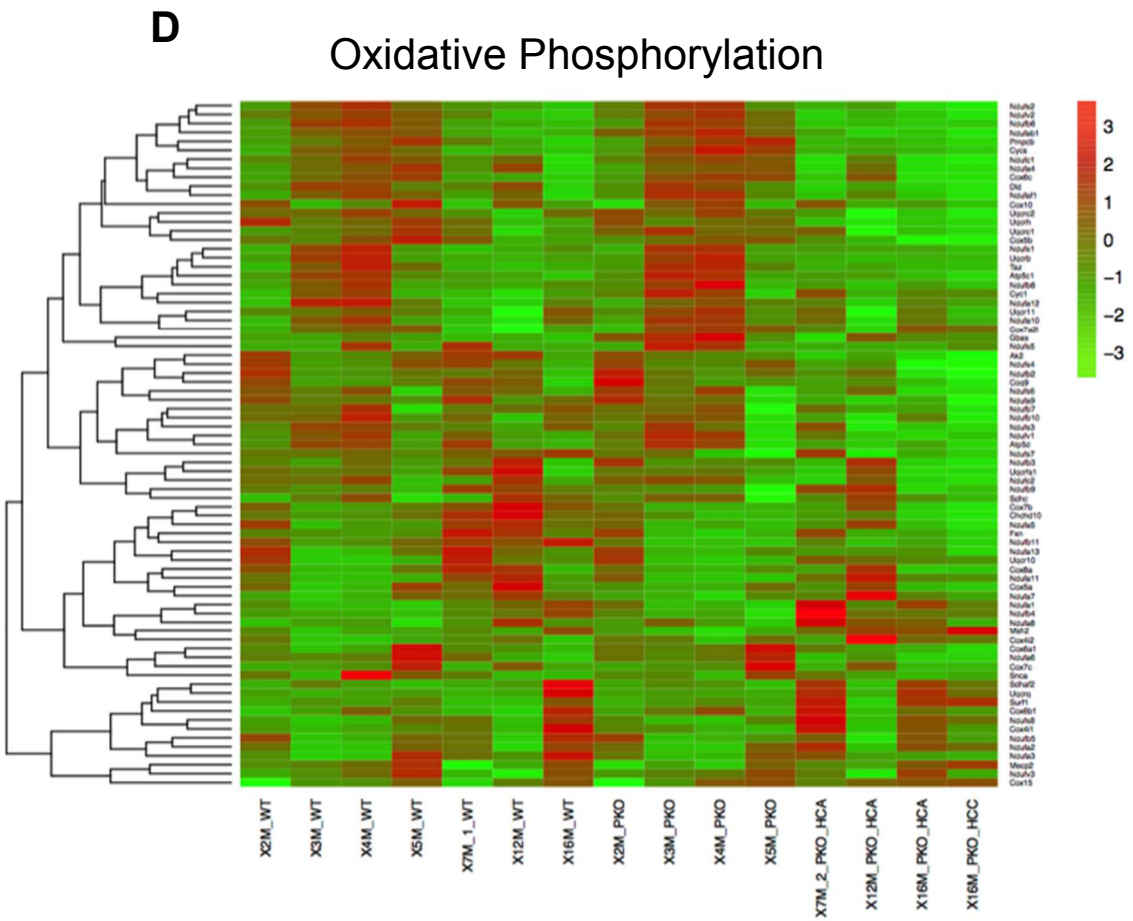

Figure 8. Mitochondrial metabolic pathways are dysregulated in PKO mice. RNA-seq analysis of mitochondrial pathways in WT and PKO mouse livers ages 2 months to 16 months. (**A**) Shows the list of metabolic pathways. Score represents relative gene expression, with a positive value indicating upregulation and a negative value indicating downregulation. High P or Low P value < 0.05 denotes gene expression is significantly upregulated or downregulated, respectively. Mitochondrial pathways that were significantly altered include (**B**) fatty acid biosynthesis, (**C**) fatty acid transport, (**D**) oxidative phosphorylation, and (**E**) amino acid catabolism. Relative gene expression is depicted by a gradient, with green representing lowest gene expression (-3) and red representing highest gene expression (+3). Genes involved in the pathway are listed to the right of the graph, continued.

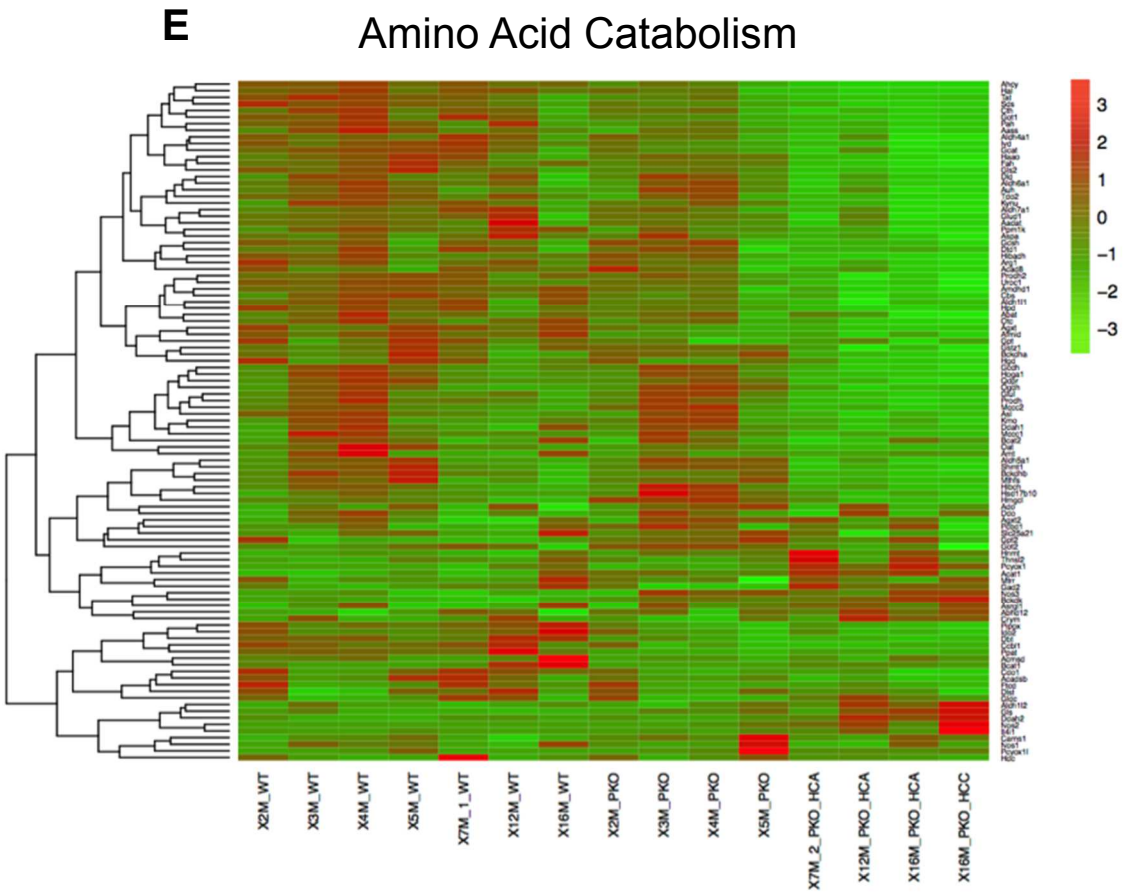

Figure 8. Mitochondrial metabolic pathways are dysregulated in PKO mice. RNA-seq analysis of mitochondrial pathways in WT and PKO mouse livers ages 2 months to 16 months. (**A**) Shows the list of metabolic pathways. Score represents relative gene expression, with a positive value indicating upregulation and a negative value indicating downregulation. High P or Low P value < 0.05 denotes gene expression is significantly upregulated or downregulated, respectively. Mitochondrial pathways that were significantly altered include (**B**) fatty acid biosynthesis, (**C**) fatty acid transport, (**D**) oxidative phosphorylation, and (**E**) amino acid catabolism. Relative gene expression is depicted by a gradient, with green representing lowest gene expression (-3) and red representing highest gene expression (+3). Genes involved in the pathway are listed to the right of the graph, continued.

Figures 1 and 2 are a reprint of the material as it appears in Dual Shp2 and Pten Deficiencies□Promote Non-alcoholic Steatohepatitis and Genesis of Liver Tumor-Initiating Cells. Luo, Xiaolin; Liao, Rui; Hanley, Kaisa L.; Zhu, Helen H.; Malo, Kirsten N.; Hernandez, Carolyn; Wei, Xufu; Varki, Nissi M.; Alderson, Nazilla; Chu, Catherine; Li, Suangwei; Fan, Jia; Loomba, Rohit; Qiu, Shuang-Jian; Feng, Gen-Sheng, *Cell Reports*, 2016. The thesis author was a co-author of this paper.

REFERENCES

Bard-Chapeau, E.A., Li, S., Ding, J., Zhang, S.S., Zhu, H.H., Princen, F., Fang, D.D., Han, T., Bailly-Maitre, B., Poli, V., Varki, N.M., Wang, H., and Feng, G.S. (2011). Ptpn11/Shp2 acts as a tumor suppressor in hepatocellular carcinogenesis. *Cancer Cell 19*, 629–639.

Chalasani, N., Younossi, Z., Lavine, J.E., Diehl, A.M., Brunt, E.M., Cusi, K., Charlton, M., and Sanyal, A.J. (2012). The diagnosis and management of nonalcoholic fatty liver disease: Practice guideline by the American Association for the Study of Liver Diseases, American College of Gastroenterology, and the American Gastroenterological Association. *Am J Gastroenterol*. 107:811–826.

Chalhoub, N., and Baker, S.J. (2009). PTEN and the PI3-kinase pathway in cancer. *Annu. Rev Pathol*. *4*, 127–150.

Chan, R. J., and Feng, G.S. (2007). PTPN11 is the first identified proto-oncogene that encodes a tyrosine phosphatase. *Blood* 109(3), 862-867.

Chih-Yin Sun, V., and Sarna, L. (2008). Symptom Management in Hepatocellular Carcinoma. *Clin J Oncol Nurs*, *12*(5), 759–766.

de Alwis, N.M.W., and Day, C.P. (2008). Non-alcoholic fatty liver disease: The mist gradually clears. *J Hepatol*. 48:S104-S112.

de La Coste, A., Romagnolo, B., Billuart, P., Renard, C.A., Buendia, M.A., Soubrane, O., Fabre, M., Chelly, J., Beldjord, C., Kahn, A., and Perret, C. (1998). Somatic mutations of the beta-catenin gene are frequent in mouse and human hepatocellular carcinomas. *Proc Natl Acad Sci U S A*. 95:8847–8851. □

Dowman, J.K., Tomlinson, J.W., and Newsome, P.N. (2009). Pathogenesis of non-alcoholic fatty liver disease. *Q J Med*. 103:71-83.

Feng, G.S. (2012). Conflicting roles of molecules in hepatocarcinogenesis: paradigm or paradox. *Cancer Cell* 21:150–154.

Fox-Walsh, K., Davis-Turak, J., Zhou, Y., Li, H., and Fu, X. D. (2011). A multiplex RNA-seq strategy to profile poly(A +) RNA: Application to analysis of transcription response and 3' end formation. *Genomics*, *98*(4), 266–271.

Galicia, V.A., He, L., Dang, H., Kanel, G., Vendryes, C., French, B.A., Zeng, N., Bayan, J.A., Ding, W., Wang, K.S., French, S., Birnbaum, M.J., Rountree, C.B., and Stiles, B.L. (2010). Expansion of hepatic tumor progenitor cells in Pten-null mice requires liver injury and is reversed by loss of AKT2. *Gastroenterology 139*, 2170–2182.

Garcia-Ruiz, I., Solis-Munoz, P., Fernandez-Moreira, D., Grau, M., Colina, F., Munoz-Yague, T., and Solis-Herruzo, J.A. (2014). High-fat diet decreases activity of the oxidative phosphorylation complexes and causes nonalcoholic steatohepatitis in mice. *Disease models & mechanisms* 7, 1287-1296.

Han, T., Xiang, D.M., Sun, W., Liu, N., Sun, H.L., Wen, W., Shen, W.F., Wang, R.Y., Chen, C., Wang, X., Cheng, Z., Li, H.Y., Wu, M.C., Cong, W.M., Feng, G.S., Ding, J., and Wang, H.Y. (2015). PTPN11/Shp2 overexpression enhances liver cancer progression and predicts poor prognosis of patients. *J Hepatology*, *63*(3), 651–660.

Iozzo, P., Bucci, M., Roivainen, A., Någren, K., Järvisalo, M. J., Kiss, J., Guiducci, L., Fielding, B., Naum, A.G., Borra, R., Virtanen, K., Savunen, T., Salvadori, P.A., Ferrannini, E., Knuuti, J., and Nuutila, P. (2010). Fatty acid metabolism in the liver, measured by positron emission tomography, is increased in obese individuals. *Gastroenterology*, *139*(3), 846–856.e6.

Kaposi-Novak, P., Lee, J.S., Gomez-Quiroz, L., Coulouarn, C., Factor, V.M., and Thorgeirsson, S.S. (2006). Met-regulated expression signature defines a subset of human hepatocellular carcinomas with poor prognosis and aggressive phenotype. *J Clin Invest*. *116*, 1582–1595.

Lade, A., Noon, L.A., and Friedman, S.L. (2014). Contributions of metabolic dysregulation and inflammation to nonalcoholic steatohepatitis, hepatic fibrosis, and cancer. *Curr Opin Oncol*. *26*, 100–107.

Lai, L.A., Zhao, C., Zhang, E.E., and Feng, G.S. (2004). The Shp-2 tyrosine phosphatase. In Protein Phosphatases, J. Arino and D. Alexander, eds. (Springer), pp. 275–299.

Lambert, J. E., Ramos-Ramos, M. A., Browning, J. D., and Parks, E. J. (2014). Increased De Novo Lipogenesis Is a Distinct Characteristic of Individuals With Nonalcoholic Fatty Liver Disease. *Gastroenterology 146*, 726–735.

Li, Y., Park, J. S., Deng, J. H., & Bai, Y. (2006). Cytochrome c oxidase subunit IV is essential for assembly and respiratory function of the enzyme complex. *J Bioenerg Biomembr*. *38*(5–6), 283–291.

Llovet J.M., Ricci S., Mazzaferro V., Hilgard P., Gane E., Blanc J.F., de Olivera, A.C., Santoro, A., Raoul, J.L., Forner, A., Schwartz, M., Porta, C., Zeuzem, S., Bolondi, L., Greten, T.F., Galle, P.R., Seitze, J.F., Borbath, I., Haussinger, D., Giannaris, T., Shan, M., Moscovici, M., Voliotis, D., and Bruix, J. (2008). Sorafenib in advanced hepatocellular carcinoma. *N Engl J Med*. 359:378–390.

Luo, X., Liao, R., Hanley, K.L., Zhu, H.H., Malo, K.N., Hernandez, C., Wei, X., Varki, N.M., Alderson, N., Chu, C., Li, S., Fan, J., Loomba, R., Qiu, S.J., and Feng, G.S.

(2016). Dual Shp2 and Pten Deficiencies Promote Non-alcoholic Steatohepatitis and Genesis of Liver Tumor-Initiating Cells. *Cell Reports* 17, 2979-2993.

King, N. (2007). Amino Acids and the Mitochondria. In *Mitochondria* (pp. 151–166).

Maeda S., Kamata H., Luo J.L., Leffert H., and Karin, M. (2005). IKKbeta couples hepatocyte death to cytokine-driven compensatory proliferation that promotes chemical hepatocarcinogenesis. *Cell* 121:977–990.

Perez-Carreras, M., Del Hoyo, P., Martin, M.A., Rubio, J.C., Martin, A., Castellano, G., Colina, F., Arenas, J., and Solis-Herruzo, J.A. (2003). Defective hepatic mitochondrial respiratory chain in patients with nonalcoholic steatohepatitis. *J Hepatol.* 38, 999-1007.

Pessaryre, D., and Fromenty, B. (2005). NASH: a mitochondrial disease. *J Hepatol*. 42: 928-940

Pikarsky, E., Porat, R.M., Stein, I., Abramovitch, R., Amit, S., Kasem, S., Gutkovich-Pyest, E., Urieli-Shoval, S., Galun, E., and Ben-Neriah, Y. (2004). NF-kB functions as a tumour promoter in inflammation-associated cancer. *Nature 431*, 461–466.

Siegel, R. L., Miller, K. D., and Jemal, A. (2016). Cancer statistics. *CA Cancer J Clin*, *66*(1), 7–30.

Takami T., Kaposi-Novak P., Uchida K., Gomez-Quiroz L.E., Conner E.A., Factor V.M., and Thorgeirsson, S.S. (2007). Loss of hepatocyte growth factor/c-Met signaling pathway accelerates early stages of N-nitrosodiethylamine induced hepatocarcinogenesis. *Cancer Res*. 67:9844–9851.

Theise, N.D. (2014). World Cancer Report 2014 IARC.

Trapnell, C., Roberts, A., Goff, L., Pertea, G., Kim, D., Kelley, D.R., Pimentel, H., Salzberg, S.L., Rinn, J.L., and Pachter, L. (2012) Differential gene and transcript expression analysis of RNA-seq experiments with TopHat and Cufflinks. *Nature Protocols* 7(3):562-578.

Wei, Y., Rector R.S., Thyfault J.P., and Ibdah, J.A. (2007). Nonalcoholic fatty liver disease and mitochondrial dysfunction. *World J Gastroenterol*. 14(2):193-199.

Youle, R.J. and van der Bliek, A.M. (2012). Mitochondrial fission, fusion, and stress. *Science* 337(6098):1062-1065.

Yu, M.C. and Yuan, J.M. (2004). Environmental factors and risk for hepatocellular carcinoma. *Gastroenterology* 127:S72–S78.

Zhang, X.F., Tan, X., Zeng, G., Misse, A., Singh, S., Kim, Y., Klaunig, J.E., and Monga, S.P.S. (2010). Conditional b-catenin loss in mice promotes chemical hepatocarcinogenesis: role of oxidative stress and platelet-derived growth factor receptor a/phosphoinositide 3-kinase signaling. *Hepatology 52*, 954–965.

Zhu, H.H., Luo, X., Zhang, K., Cui, J., Zhao, H., Ji, Z., Zhou, Z., Yao, J., Zeng, L., Ji, K., Gao, W.Q., Zhang, Z.Y., and Feng, G.S. (2015). Shp2 and Pten have antagonistic roles in myeloproliferation but cooperate to promote erythropoiesis in mammals. *Proc Natl Acad Sci. USA 112*, 13342–13347.

Zucman-Rossi, J., Villanueva, A., Nault, J.C., and Llovet, J.M. (2015). Genetic landscape and biomarkers of hepatocellular carcinoma. *Gastroenterology 149*, 1226–1239.e4.